2011

Zn13(CrxAl1–x)27 (x = 0.34–0.37): a new intermetallic phase containing icosahedra as building units

Srinivasa Thimmaiah
Iowa State University

Mi-Kyung Han
Iowa State University

Gordon J. Miller
Iowa State University, gmiller@iastate.edu

Zn13(CrxAl1−x)27 (x = 0.34–0.37): a new intermetallic phase containing icosahedra as building units

Abstract
The title compounds $Zn_{13}(Cr_xAl_{1-x})_{27}$ (x = 0.34–0.37) were obtained by melting the pure elements at 923 K, and followed by a heat treatment at 723 K in a tantalum container. According to single crystal structural analysis, the title compounds crystallize in the rhombohedral system, adopting a new structure type (R-3m, a = 7.5971(8), c = 36.816(6), for crystal **I**). Single crystal X-ray structural analysis reveals a statistical mixing of Cr/Al in their crystallographic positions. Single crystal and powder X-ray diffraction as well as energy dispersive X-ray analyses suggested the title phase to have a narrow homogeneity range. The substructure of $Zn_{13}(Cr_xAl_{1-x})_{27}$ shows close resemblance with the Mn_3Al_{10} structure type. A bonding analysis, through crystal orbital Hamiltonian populations (COHPs), of "$Cr_9Al_{18}Zn_{13}$" as a representative composition indicated that both homo- and heteronuclear interactions are important for the stability of this new phase.

Keywords
intermetallic compound, I3 cluster, single crystal structure analysis, powder diffraction analysis, x-ray diffraction

Disciplines
Materials Chemistry | Other Chemistry | Physical Chemistry

Comments
This article is from *Zeitschrift für Kristallographie - Crystalline Materials* 226 (2011): 557, doi:10.1524/zkri.2011.1376. Posted with permission

Z. Kristallogr. **226** (2011) 557–567 / **DOI** 10.1524/zkri.2011.1376

$Zn_{13}(Cr_xAl_{1-x})_{27}$ ($x = 0.34–0.37$): a new intermetallic phase containing icosahedra as building units

Srinivasa Thimmaiah*, Mi-Kyung Han and Gordon J. Miller

Iowa State University and Ames Laboratory, US Department of Energy Ames, Iowa 50011, USA

In memoriam Professor Dr. Dr. h.c. mult. Hans-Georg von Schnering

Received January 7, 2011; accepted March 13, 2011

Intermetallic compound / I3 cluster / Single crystal structure analysis / Powder diffraction analysis / X-ray diffraction / Complex

Abstract. The title compounds $Zn_{13}(Cr_xAl_{1-x})_{27}$ ($x = 0.34–0.37$) were obtained by melting the pure elements at 923 K, and followed by a heat treatment at 723 K in a tantalum container. According to single crystal structural analysis, the title compounds crystallize in the rhombohedral system, adopting a new structure type ($R\bar{3}m$, $a = 7.5971(8)$, $c = 36.816(6)$, for crystal **I**). Single crystal X-ray structural analysis reveals a statistical mixing of Cr/Al in their crystallographic positions. Single crystal and powder X-ray diffraction as well as energy dispersive X-ray analyses suggested the title phase to have a narrow homogeneity range. The substructure of $Zn_{13}(Cr_xAl_{1-x})_{27}$ shows close resemblance with the Mn_3Al_{10} structure type. A bonding analysis, through crystal orbital Hamiltonian populations (COHPs), of "$Cr_9Al_{18}Zn_{13}$" as a representative composition indicated that both homo- and heteronuclear interactions are important for the stability of this new phase.

Introduction

Quasicrystals (QCs) are a fascinating class of intermetallic compounds, which have become an interesting area of research for chemists and physicists since their discovery in the Al–Mn system [1]. These complex intermetallic compounds exhibit forbidden rotational symmetries, *e.g.*, 5-, 8-, 10- and 12-fold, in their diffraction patterns and they lack three-dimensional translational atomic periodicity [2, 3]. Over the past two decades, numerous studies have focused on the discovery of new QCs and their closest crystalline relatives, so-called approximants, in a variety of binary, ternary, and quaternary systems. The crystalline approximants (CAs) are periodic and their local atomic structure and physical properties, in general, closely resemble the parent high-symmetry QCs. Icosahedral approximants (iCAs) are categorized based on their local atomic order and cluster arrangements, such as the Bergman- [4], Mackay [5], and Tsai-type phases [6]. Icosahedra and dodecahedra are the common building blocks for all these different types of phases.

All of these QCs and CAs are generally recognized as *electron phases* or *Hume-Rothery phases* because they occur for a specific range of valence electron concentrations (*vec*) 1.75–2.10 e^-/atom, and their structural stability can be rationalized by an interaction of the nearly free electron Fermi surface and Brillouin zone planes in reciprocal space [7, 8]. A similar structural stability concept also holds for the γ-brass and related structures [9]. Recently, S. Lee *et al.,* beautifully showed the connections of Laves phases, γ-brasses, and $2 \times 2 \times 2$ superstructures of γ-brasses to QCs by using a higher dimensional approach [10, 11]. In addition, new icosahedral QCs have been discovered in Cd-based [12–14], Mg–Zn-based [15–17] and Au–In based [18] alloys. Some of these were uncovered by using choosing chemical compositions based on tuning the valence electron count to a pseudogap in the electronic density of states (DOS) curve of a corresponding CA [16, 18]. All of these findings motivate us to find new structural families consisting of icosahedra as the main building block that can eventually lead to improved understanding of the structural features of QCs and their CAs.

The binary Cr–Al system has been studied by many authors over the several decades because of the existence of numerous structurally complex phases in a small cascade on the Al-rich side of the phase diagram [18–21]. For instance, $CrAl_7$, Cr_2Al_{11}, μ-$CrAl_4$, ε-$CrAl_4$ and γ-Cr_5Al_8, are few of the known complex phases that exist in this region. The μ-$CrAl_4$ phase is isostructural to μ-$MnAl_4$, one of the CAs in the Al–Mn system [22]. The complex structure of μ-$MnAl_4$ along with other structurally complex phases have been described using the *I*3-cluster concept developed by Kreiner and Franzen [23]. Moreover, several CA structures have also been discovered in ternary TM-Cr–Al systems [TM=Mn, Fe, Ni] [24–27].

On the other hand, the Cr–Zn system is much less studied, with only the zinc-rich part of the phase diagram available [28, 29]. The only reported phase in this system

* Correspondence author (e-mail: srini@iastate.edu)

is $CrZn_{17}$, which apparently crystallizes in the hexagonal system, but its crystal structure remains unknown [30]. In addition, "$CrZn_{13}$" has been mentioned to be isotypic with ζ-$FeZn_{13}$ [28, 31], but the structural characterization is highly incomplete [32]. A thermodynamic assessment of the zinc-rich part of the Cr–Zn system was carried out by G. Reumont *et al*. In addition, they also optimized the Cr–Al–Zn system with the *CALPHAD* method [33], after probing this system experimentally and reporting four ternary phases, which they labeled τ_1 (Zn-rich), τ_2 and τ_3 (Al-rich), and τ_4 (Cr-poor) [33]. However, no structural details were given of any of these proposed ternary phases.

This work involves a part of our effort devoted to understanding the role of *vec* and electronic structure of complex intermetallic structures that have structural relationships to QCs, *e.g.*, γ-brass type phases. We recently demonstrated that partial substitution of Al, a *sp* metal, for Zn in the aristotypic γ-$Pd_{2-x}Zn_{11+x}$ leads to either a γ-brass or a $2 \times 2 \times 2$ superstructure of γ-brass type phases, depending on Al content, in the Pd–Zn–Al ternary system [34]. In addition, we reported the structural and magnetic characteristics of the binary series, MGa (M = Cr, Mn, Fe), and pseudobinary series, $Cr_{1-x}Fe_xGa$, both of which adopt the rhombohedral Cr_5Al_8 structure type [35, 36]. This structure is, in fact, a distorted γ-brass type structure. Thus, we undertook an exploration of the Cr–Al–Zn ternary system to continue our search for new CAs and iCAs, as well as icosahedral QCs, for a better understanding of their structure-composition relationships. Herein, we report our initial fruitful results in the Al/Zn-rich part of the Cr–Zn–Al phase diagram.

Experimental section

Synthesis

The title compounds were synthesized starting from the pure elements: Cr (chunks, MPC, Ames Laboratory, 99.98%), Zn (ingot, MPC, Ames Laboratory, 99.99%), Al (tear drop, MPC, Ames Laboratory, 99.99%). The new phase was initially identified during exploratory synthesis from the loaded composition in the molar ratio Cr : Zn : Al = 1 : 2 : 2. The reactants were placed in a Ta tube, which was crimped shut and sealed within a fused silica ampoule under vacuum, heated continuously from room temperature to 650 °C at a rate of 15 °C/hr in a tube furnace and held for 12 hrs. Thereafter, the furnace was slowly cooled to 450 °C over a period of 12 hrs, and equilibrated at this temperature for 7 days. Finally, the furnace was turned off and allowed to cool naturally to ambient temperature. The product contained a mixture of title compound (major, >90%), Cr_5Al_8 (minor), and a small amount of Zn condensed on the cooler part of the silica tube. The major phase showed characteristic silvery rhombic facets, and these are easily extracted for single crystal diffraction experiments. Further loadings were carried out in the vicinity of the composition refined from single crystal diffraction studies and EDS analysis ($Cr_{22(1)}Zn_{34(1)}Al_{44(1)}$). Ca. 0.5 g samples of precisely weighed metals were loaded into cleaned tantalum tubes as reaction containers, each of which was crimped and then sealed in a silica jacket under reduced pressure (ca. 10^{-5} torr).

The more rigorous syntheses were carried out using different temperature profiles in order to optimize the reaction conditions to obtain maximum yield of the title phase. For instance, when mixtures were heated to 850 °C for 12 h to homogenize them, followed by cooling to 450 °C over the period of 14 h, we observed reaction with the Ta tubes resulting in embrittlement of the tube. However, no Ta was observed in the EDS analysis of the final product. The product thus obtained showed a second, minor phase, $(Cr,Al)_3Zn$, along with Cr_5Al_8 and the title phase (see discussion). The following reaction temperature profile was ultimately chosen because these conditions gave high yields of all title phases and good quality crystals for diffraction experiments. The reaction containers were heated continuously from room temperature to 650 °C at a rate of 15 °C/hr in a tube furnace and held for 12 hrs; thereafter, the furnace was slowly cooled to 450 °C over a period of 12 hrs, and equilibrated at this temperature for 7 days. Finally, the furnace was turned off and allowed to cool naturally to ambient temperature. Our exploration of this Cr/Zn/Al phase space indicated that the title phase formed as the major phase when the molar composition of Cr ranged between 20 and 36 percent. Since the mixture of Zn and Al is, therefore, in excess, it acts like a reactive flux that facilitates crystal growth of the desired phase.

For phase purity and verification of any homogeneity range, all samples were characterized by powder X-ray diffraction using a Huber G670 imaging plate Guinier camera equipped with a Ge(111) monochromator with CuK_{α_1} radiation. Patterns were collected for 2θ values ranging from 5° to 100° at increments of 0.005°. A few samples were also investigated by using the Philips PANalytical X′Pert PRO diffractometer. The data were collected for 2θ values ranging 5° to 90° at increments of 0.02° in a continuous scan mode using CuK_α radiation in a Bragg-Brentano geometry. The lattice parameters were evaluated using the Rietveld refinement module of the PANalytical X-Pert Highscore Plus software (PANalytical, version 2.1). The refined lattice parameters corroborate well with lattice parameters obtained from the single crystal diffraction experiments.

Semiquantitative microprobe analyses were performed on flat surfaces of several single crystals using a JEOL 5910LV scanning electron microscope (SEM) equipped with a Noran-Vantage energy-dispersive spectrometer. The chemical compositions obtained from energy dispersive X-ray analysis (EDS) corroborate well with single crystal data analysis, within the limitations of the technique. No heavy elements other than Cr, Zn, and Al were detected. For phase identification, images were taken in the back-scattered electron mode at 20 kV on the same instrument.

Single crystal structure determination

At least eight crystals extracted from different loaded compositions were studied with a Bruker APEX CCD diffractometer equipped with graphite-monochromatized MoK_α radiation ($\lambda = 0.71073$ Å). Reflections were gathered at room temperature by taking three sets of 606 frames with

0.3° scans in ω, with an exposure time of 10 s per frame using the *SMART* program [37]. The range of 2θ extended from 4 to 57°. The measured intensities were corrected for Lorentz and polarization effects and were further corrected for absorption using the STOE *X-SHAPE* [38] and *X-RED* programs [39]. All data sets showed the systematic absence condition, *hkl:* $-h + k + l = 3n$, etc., which suggests rhombohedral symmetry and five possible space groups, $R\bar{3}$, $R3$, $R3m$, $R32$, and $R\bar{3}m$. The E-Stats model strongly suggested the structure to be centrosymmetric; so the space group was tentatively selected to be $R\bar{3}m$.

The structural models were obtained from direct methods and refined by full-matrix, least-squares refinement on F^2 using the *SHELXTL* package [40]. Direct methods yielded nine distinct atomic positions. Among them, three positions are assigned to Zn and the remaining sites to Cr on the basis of the thermal displacement parameters. The subsequent isotropic least-squares refinement for crystal **I** (loaded composition $CrAl_2Zn_2$) converged quickly to $R1 = 8.63\%$, $wR2 = 29.5\%$, at which point no meaningful residual electron density was seen in the difference Fourier map ($<3.0\ e^-/Å^3$). However, all Cr atoms showed large thermal displacement parameters ($0.018-0.022\ Å^2$), which suggested that either Al atoms may partially mix with Cr at similar crystallographic positions or there may be vacancies disordered among these Cr positions. In the following refinement cycles, all the Cr positions were treated as mixed with Al atoms (site occupancy factor (sof) constrained to unity). As a result, the $R1$ and $wR2$ factors dropped to 5.08 and 12.48%, respectively. Introduction of anisotropic displacement parameters and a secondary extinction coefficient during the final stage of refinement yielded $R1 = 3.65\%$ for 51 parameters. Standardization of the atomic positions was performed with STRUCTURE TIDY as implemented in the *WinGX* software package [41]. In order to check any homogeneity range for the new structure, several crystals were also selected from different loading compositions; however crystal **II** (loaded composition $CrAlZn_2$) showed maximum incorporation of Cr compared to the others. The isotropic least-squares refinement for crystal **II** showed characteristics similar to that of crystal **I**, *i.e.*, mixed Cr and Al position. Tables 1 and 2 summarize atomic positions, site occupancy factors, and displacement parameters for crystals **I** and **II**[1].

Electronic structure calculations

To assess chemical bonding factors leading to the existence of the title compounds, a theoretical electronic structure for the model compound, "$Cr_9Al_{18}Zn_{13}$", using the crystallographic results above were calculated using the tight-binding, linear muffin-tin orbital (TB-LMTO) method in the atomic spheres approximation (ASA) [42–45] by the Stuttgart code. Exchange and correlation were treated in the local density approximation [46]. All relativistic effects except spin-orbit coupling were taken into account using a scalar relativistic approximation [47]. In the ASA, space is filled with small, overlapping Wigner-Seitz (WS) spheres at each atomic site. The symmetry of the potential is considered to be spherical inside each WS sphere, and a combined correction takes into account the overlapping part [48]. The radii of the WS spheres were obtained by requiring that the overlapping potential be the best possible approximation to the full potential, and were determined by an automatic procedure [48]. No empty spheres were needed to satisfy the LMTO overlap criterion. The corresponding WS radii for the various atoms include the following ranges: Cr, 1.550–1.670 Å; Zn, 1.391–1.608 Å; and Al, 1.488–1.666 Å. The basis set included Cr 4*s*, 4*p*, and 3*d* orbitals, Zn 4*s*, 4*p*, and 3*d* orbitals, and Al 3*s*, 3*p* and 3*d* orbitals. The ***k***-space integrations to determine the self-consistent charge density, densities of states (DOS) and crystal Hamiltonian orbital populations (COHP) [49] were performed by the tetrahedron method [50]. The self consistent charge density was obtained using 288 irreducible ***k***-points in the irreducible wedge of the rhombohedral Brillouin zone.

Results and discussion

The identified phases based on powder X-ray diffraction (PXRD) intensity profile analysis on various samples are summarized in Table 1. Most specimens showed multiple phases by PXRD as well as EDS. Several attempts were made to obtain single phase samples by varying the loading compositions in the vicinity of the composition obtained from X-ray single crystal diffraction experiments, as well as choosing different heat treatments. No single phase sample was observed, either by prolonged annealing at 450 °C, or by quenching the reaction mixture from 650 °C. In all cases, the final product mainly consists of the title phase (yield $> 85\%$ as estimated from PXRD) and a small amount of Cr_5Al_8. According to PXRD intensity fitting, the estimated amount of the Cr_5Al_8 phase is found to be ca. 5–15%. EDS analysis of several samples also confirm the presence of this Cr_5Al_8 phase. Cr_5Al_8 adopts a rhombohedrally distorted γ-brass type structure. In addition, the Cr_5Al_8 phase shows variation in its lattice parameters (see Table 1). These changes could be due to the homogeneity range for the Cr_5Al_8 phase or a small amount of Zn incorporation into the parent Cr_5Al_8 structure. The presence of Zn in the parent Cr_5Al_8 phase could not be confirmed from single crystal diffraction studies due to the poor crystalline quality of this minor product. Nevertheless, EDS analysis on several crystals does indicate the presence of small amount of Zn, *e.g.*, $Cr_{35}Al_{61}Zn_4$. However, this level of Zn detected from EDS analysis falls under the detection limitations of the instrument, so we have ruled out the possibility of Zn being incorporated into the Cr_5Al_8 structure.

The top panel of Fig. 1 shows a typically observed PXRD pattern of the product obtained from a sample heated to 850 °C, and followed by heat treatment at 450 °C for 5 days. The bottom panels show the calculated powder patterns from their identified phases. The powder patterns obtained under these conditions show a mixture of

[1] Further details of the structure determinations may be obtained from: Fachinformationszentrum Karlsruhe, 76344 Eggenstein-Leopoldshafen, Germany by quoting the Registry No's. CSD-422616 [$Zn_{13}Cr_{9.22}Al_{17.78(1)}$(**I**)], and CSD-422617 [$Zn_{13}Cr_{9.87}Al_{17.13(2)}$(**II**)].

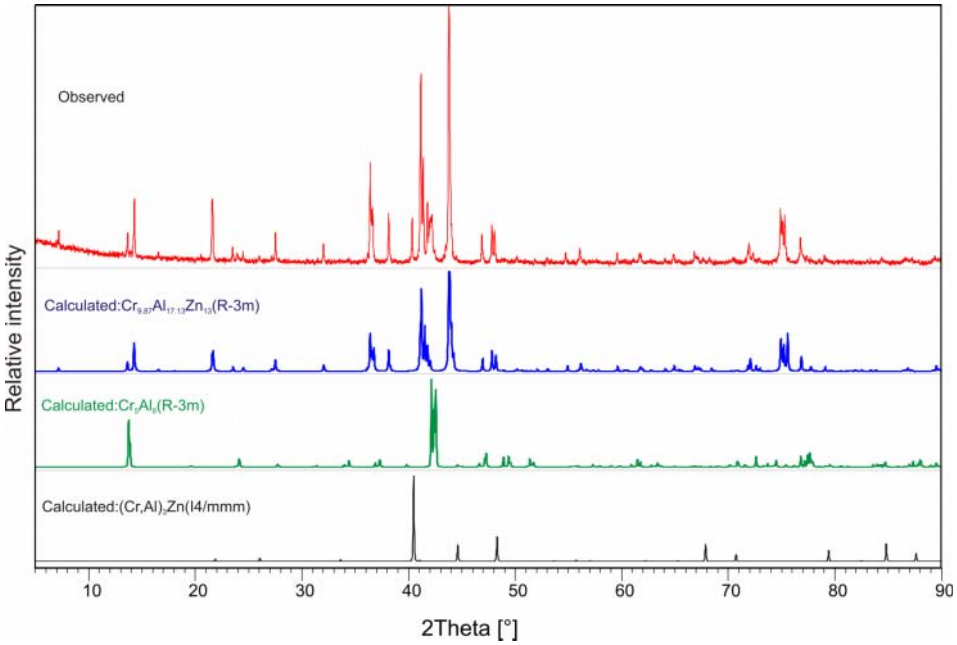

Fig. 1. X-ray diffraction pattern (top) obtained for the loaded composition $Cr_{25}Al_{25}Zn_{50}$, prepared at 850 °C, and followed by heat treatment at 450 °C for 5 days. Bottom panels show the calculated intensities from the three identified phases-the title phase $Zn_{13}(Cr_xAl_{1-x})_{27}$ with maximum yield ca. 87% and followed by Cr_5Al_8 (yield ca. 8%) and $(Cr,Al)_3Zn$ (yield ca. 5%).

three phases. According to an analysis of the intensity profiles, the product consists of the title phase (yield ca. 87%), along with two other minor phases, namely, Cr_5Al_8 (yield ca. 8%) and $(Cr,Al)_3Zn$ (yield ca. 5%). The $(Cr,Al)_3Zn$ phase was observed in small yield when the reaction temperature achieved at least 850 °C. Although the yield of the $(Cr,Al)_3Zn$ phase is small, its crystals can be easily hand-picked with the help of an optical microscope, since they show a distinct morphology (see Fig. 1b). The crystal structure was solved in the tetragonal space group *I*4/*mmm,* and the composition refined to be $Cr_{1.80(3)}Al_{1.20}Zn$ ($a = 3.7806(2)$ Å and $c = 8.1373(8)$ Å). Figure 2 shows the SEM images of the three phases in back-scattered electron mode. The phase contrast between Cr_5Al_8 and $(Cr,Al)_3Zn$ can be clearly seen in Fig. 2b.

The crystal structure of the title phase, $Zn_{13}(Cr_xAl_{1-x})_{27}$ represents a new structure type (space group $R\bar{3}m$). The unit cell volume accommodates 120 atoms (Pearson code *hR*120), which are distributed over 9 crystallographically distinct sites. Among them, three sites are exclusively occupied by Zn atoms (Wyckoff sites 3*b*, 18*h*, and 18*h*), and the remaining six sites show statistically mixed Cr and Al atoms (see Table 2). Refined compositions yielded a small range of Cr content to be $0.34 \leq x \leq 0.37$. All structural refinements on several crystalline specimens show no evidence of mixing between Zn and Cr or Al atoms.

Table 1. Loaded compositions, obtained products, and refined lattice parameters. For many reactions, a small amount of Al/Zn condensed on the cooler part of the silica tube. Crystals are selected from samples (1) and (2) for single crystal diffraction studies. The descriptors, "major" and "minor", indicate qualitative relative intensities of the highest reflection for each phase listed.

	Loaded composition			Refined lattice Parameters (Å)
	Cr	Al	Zn	
1	20	40	$40^{(1)}$	$a = 7.5971(8)$ $c = 36.816(6)$ (major)[a]
	EDS : $Cr_{23(1)}Al_{43(1)}Zn_{34(1)}$			$a = 12.872(1)$, $c = 7.7831(8)$ (minor)[b]
				$a = 7.5961(1)$, $c = 36.9487(6)$ (major)[a]
2	20	30	$50^{@}$	$a = 12.8709(9)$, $c = 7.7802(7)$ (minor)[b]
				$a = 3.7771(5)$, $c = 8.133(2)$ (minor)[c]
3	23	44.5	32.5	$a = 7.5993(2)$, $c = 36.966(1)$ (major)[a]
				$a = 12.8995(7)$, $c = 7.8389(4)$ (minor)[b]
4	25	25	$50^{(2)@}$	$a = 7.6084(15)$, $c = 37.076(10)$ (major)[a]
	EDS : $Cr_{25(1)}Al_{45(1)}Zn_{30(1)}$)			$a = 12.9008(4)$, $c = 7.8389(4)$ (minor)[b]
				$a = 3.7746(3)$, $c = 8.1286(9)$ (minor)[c]
5	30	20	50	$a = 7.5965(1)$, $c = 36.9572(8)$ (major)[a]
				$a = 12.8726(6)$, $c = 7.8150(5)$ (minor)[b]
6	33	33	34	$a = 7.5931(2)$, $c = 36.9362(9)$ (major)[a]
				$a = 12.9017(6)$, $c = 7.8430(6)$ (minor)[b]
7	36	45	39	$a = 7.5962(2)$, $c = 36.962(1)$ (major)[a]
				$a = 12.943(1)$, $c = 7.6863(8)$ (minor)[b]

a: title phase; b: Cr_5Al_8 ($R\bar{3}m$); c: $(Cr,Al)_3Zn$ (*I*4/*mmm*); @: Reaction carried out at 850 °C and followed by heat treatment at 450 °C for 5 days.

Table 2. Crystal data and structural refinement for $Zn_{13}(Cr_xAl_{1-x})_{27}$ ($x = 0.34–0.37$).

	Crystal **I**	Crystal **II**
Compound	$Zn_{13}Cr_{9.22}Al_{17.78(1)}$	$Zn_{13}Cr_{9.87}Al_{17.13(2)}$
Crystal system	Rhombohedral	Rhombohedral
Space group	$R\bar{3}m$	$R\bar{3}m$
Unit cell dimensions Å	$a = 7.5971(8)$	$a = 7.6084(15)$
	$c = 36.816(6)$	$c = 37.076(10)$
Volume (Å^3); Z	1840.2(4); 3	1858.7(7); 3
$\varrho_{X\text{-ray}}$(g cm^{-3}); μ (cm^{-1})	4.897; 16.963	4.892; 17.038
Diffractometer	Bruker CCD	
Radiation; wavelength	MoK_α; $\lambda = 0.71073$ Å	
Crystal size (mm^3)	$0.14 \times 0.06 \times 0.04$	$0.12 \times 0.07 \times 0.05$
2θ-range (°)	$2\theta < 56.2°$	
hkl-range	$-9 \le h \le 9$, $-10 \le k \le 10$, $-48 \le l \le 48$	$-10 \le h \le 10$, $-10 \le k \le 9$, $-48 \le l \le 48$
No. Reflections; $R_{int.}$	7241; 0.0353	5455; 0.0783
No. independent reflections	625	621
No. Parameters	51	50
Absorption correction	Numerical	Numerical
Goodness-of-fit on F^2	1.044	1.130
Final R indices [$I > \sigma(I)$]	$R1 = 0.0365$, $wR2 = 0.0951$	$R1 = 0.0466$, $wR2 = 0.1121$
R indices (all data)	$R1 = 0.0391$, $wR2 = 0.0965$	$R1 = 0.0546$, $wR2 = 0.1194$
Extinction coefficient	0.00019(6)	–
Largest diff. peak and hole	1.351 and -1.563 e$^-$/Å^3	1.456 and -1.432 e$^-$/Å^3

The most prominent features of this new crystal structure are two distinct atom-centered icosahedra built around the Zn1 and M1 sites. Figure 3 depicts two polyhedral representations of the structure of $Zn_{13}(Cr_xAl_{1-x})_{27}$, viewed along the [110] direction. The Zn1-centered icosahedron has six Zn3 nearest neighbors at 2.5379 Å and six M4 atoms at 2.683 Å: Zn1@6Zn3+6M4. Furthermore, the M1-centered icosahedron has six Zn2 nearest neighbor at 2.5379 Å and six M3 at 2.683 Å: M1@6Zn2+6M3. These icosahedra are stacked along the crystallographic c-axis in a $\cdots$ABC$\cdots$ pattern, as depicted in Fig. 3 (left). Additionally, each of the M1-centered icosahedra is surrounded by a slightly distorted pentagonal dodecahedron formed by three Cr/Al sites, which sit above every face of the inner icosahedron: M1@(6Zn2+6M3)(12M5+6M6+2M2). The distance between the central M1 site to the peripheral atoms of the dodecahedron range from 4.202(3) Å to 4.314(2) Å, as depicted in Fig. 3 (right). The dodecahedra are condensed along the crystallographic a and b directions by sharing common edges (M5 atoms) forming a 2D network. However, there is no condensation of these polyhedra along the c direction because the Zn1-centered icosahedra are present between the layers. Figure 4 shows the coordination polyhedra of the nine sites in the asymmetric unit. Interatomic distances are listed in Table 3. Zn1, Zn2 and M1 sites are surrounded by nearly regular icosahedra. The coordination polyhedron of Zn3 is a truncated icosahedron with coordination number 11 (CN11). A bicapped pentagonal prism is found surrounding the M4 and M5 sites. Finally, the M2 and M6 sites exhibit more regular coordination polyhedra of CN12, and the M3 site has a coordination polyhedron of CN13.

The substructure of M1-centered nested polyhedra shows a close resemblance to the Mn_3Al_{10} structure,

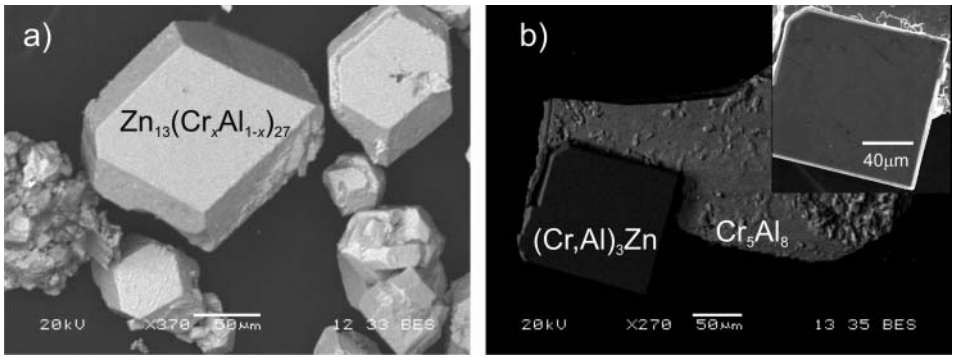

Fig. 2. SEM micrographs in back-scattered electron mode at two different regions for the loaded composition $Cr_{25}Al_{25}Zn_{50}$. **(a)** Major phase displaying rhombic crystal morphology. **(b)** Two other minor phases, the Cr_5Al_8 phase and the $(Cr,Al)_3Zn$ phase showing the rectangular morphology of the tetragonal phase. Inset: SEM image of the tetragonal phase in secondary electron mode.

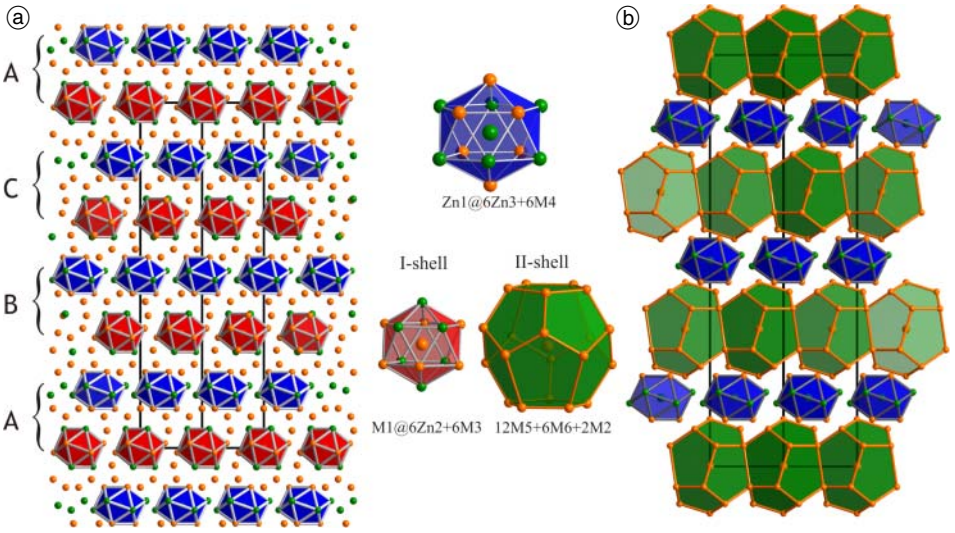

Fig. 3. [110] Projection of the $Zn_{13}(Cr_xAl_{1-x})_{27}$ structure. **(a)** Layers of icosahedra around Zn1 (blue) and M1 (red) atoms stacked along the *c* direction in a $\cdots$ABCABC$\cdots$ manner. **(b)** Highlighting the dodecahedra surrounding the M1-centered icosahedra, which are omitted for the clarity.

which is a 3D network. Thus, the main difference between $Zn_{13}(Cr_xAl_{1-x})_{27}$ and Mn_3Al_{10} is the presence of an additional layer of isolated Zn1-centered icosahedra between these nested polyhedra that give rise to a 2D network in $Zn_{13}(Cr_xAl_{1-x})_{27}$ rather than a 3D network Mn_3Al_{10} (see Fig. 3 (right) and Fig. 6). In addition, this substructure is also observed in the rhomobohedrally distorted γ-brass structures, *e.g.*, MnGa and Cr_5Al_8. In analogy to the Mn_3Al_{10} structure, an alternative and elegant way of describing these new structures is to separate the atoms of $Zn_{13}(Cr_xAl_{1-x})_{27}$ into puckered (*P*-) and flat (*F*-)layers that are stacked along *c* direction. Six *F*- and twelve *P*-layers per unit cell are stacked along *c*-axis with the sequence $\cdots PFPFPP\cdots$ (×3) as shown the Fig. 5; in Mn_3Al_{10}, we recognize a stacking sequence of $\cdots PFPF\cdots$ per unit cell. In $Zn_{13}(Cr_xAl_{1-x})_{27}$, the two puckered layers exhibit the same tiling pattern, Schläfli symbol $(3^6)^1$; $(3^2434)^6$, but have different chemical compositions. One-fourth of the *P*-layers consists of only Zn atoms (green layers in Fig. 5), while three-fourths of them contain a mixture of Cr and Al atoms (orange layers in Fig. 5). The *F*-layers, Schläfli symbol $(3939)^1$; $(3^39)^1$, are structurally equivalent, and, therefore, adopt a single composition containing all three elements. In Mn_3Al_{10}, the *F*- and *P*-layers have identical tilings, see Fig. 6.

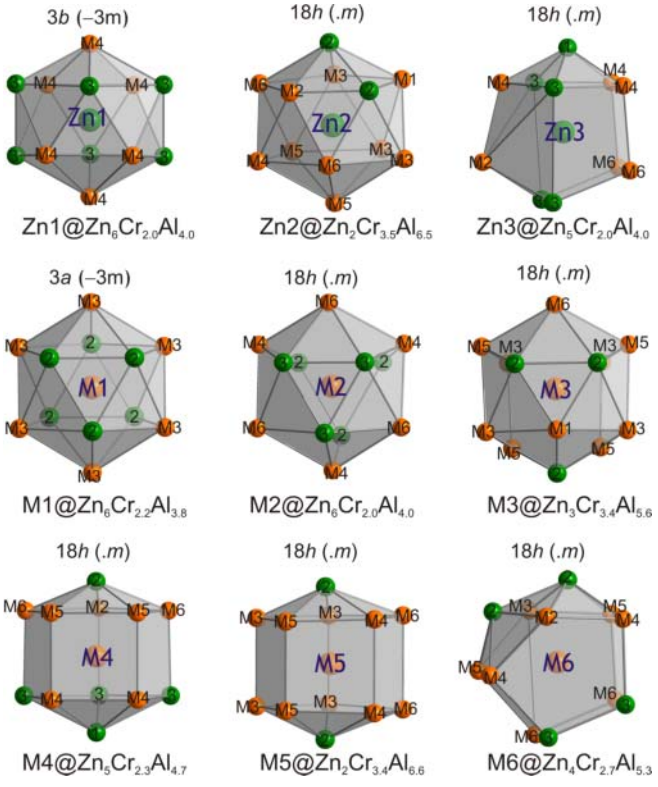

Fig. 4. Coordination polyhedra around the different sites in the asymmetric unit for **crystal I**. The orange and green spheres represent, Cr/Al (M) and Zn atoms, respectively.

A more effective way of describing this new structure, however, is by using the *I*3-cluster concept, in which the *I*3-cluster consists of three vertex-connected icosahedra. This concept has been effectively adopted to describe complex structures which are CAs. For instance, λ-$MnAl_4$ [51], κ-$Ni_6Cr_{18}Al_{76}$ [52], $Ga_{12+x+y}Mg_{11-y}Pd_{6-x}$ [53], γ-$AgMg_4$ [54], and Ir_9Al_{28} [55] have *I*3-clusters each with different connectivities as described by Kreiner and Franzen [23]. They identified four different types of *I*3-cluster connectivity in different structures: (i) *B*-type (bridge-type); (ii) *I*-type (interpenetrating-type); (iii) *S*-type (sharing-type); and (iv) *L*-type (a cluster of four icosahedra at the corners of a tetrahedron). In the $Zn_{13}(Cr_xAl_{1-x})_{27}$ structure we identified *B*-type, *I*-type, and *L*-type modes of *I*3-cluster connectivity as highlighted in Fig. 7 (left and center).

Interpenetrating icosahedra (*I*-type) occur at the Zn2 sites, which form a triangular arrangement in each *F*-layer. Each Zn2 site has two Zn2 nearest neighbors arranged in a triangle at a separation of ca. 2.671 Å. These triangles form a 2D network of vertex-connected and interpenetrating icosahedra (*I*-type) with two *P*-layers located above and below the *F*-layer. The building block is three vertex-connected icosahedra, *i.e.*, an *I*3-cluster, which are basically found in the sequence of $\{\cdots PFP\cdots\}$ layers. The additional icosahedra centered by Zn1 atoms located in the *P*-layer (green layer) share common vertices with *I*3-clusters located in the $\{\cdots PFP\cdots\}$ layers to form a building block of four vertex-connected icosahedra, using M4 connecting atoms. This connectivity is known in terms of the

Table 3. Atomic coordinates and equivalent isotropic displacement parameters for crystals **I** and **II**. U_{eq} is defined as one-third of the trace of the orthogonalized U_{ij} tensor.

Atom	Wyck.	Occ.	*x*	*y*	*z*	U_{eq}
Zn1	3*b*	1	0	0	1/2	0.013(1)
		1	***0***	***0***	***1/2***	***0.014(1)***
Zn2	18*h*	1	0.5494(1)	0.4505(1)	0.2786(1)	0.013(1)
		1	***0.5498(1)***	***0.4502(1)***	***0.2776(1)***	***0.014(1)***
Zn3	18*h*	1	0.5456(1)	0.4544(1)	0.1532(1)	0.014(1)
		1	***0.5456(1)***	***0.4544(1)***	***0.1532(1)***	***0.015(1)***
M1	3*a*	0.40(3)*	0	0	0	0.008(1)
		0.36(4)*	***0***	***0***	***0***	***0.011(2)***
M2	6*c*	0.38(2)*	0	0	0.1141(1)	0.010(1)
		0.40(3)*	***0***	***0***	***0.1148(1)***	***0.009(1)***
M3	18*h*	0.37(1)*	0.4663(1)	0.5337(1)	0.3468(1)	0.011(1)
		0.50(2)*	***0.4656(2)***	***0.5344(2)***	***0.3471(1)***	***0.014(1)***
M4	18*h*	0.34(1)*	0.4582(1)	0.5418(1)	0.2189(1)	0.010(1)
		0.27(2)*	***0.4581(2)***	***0.5419(2)***	***0.2187(1)***	***0.009(1)***
M5	18*h*	0.31(1)*	0.4585(1)	0.5415(1)	0.0501(1)	0.010(1)
		0.37(2)*	***0.4581(2)***	***0.5419(2)***	***0.0504(1)***	***0.012(1)***
M6	18*h*	0.32(1)*	0.7931(1)	0.2069(1)	0.0909(1)	0.011(1)
		0.31(2)*	***0.7928(2)***	***0.2072(2)***	***0.0911(1)***	***0.011(1)***

M = Cr/Al, * = SOF of Cr, Al = 1 − SOF of Cr

*I*3-cluster concept as an *L*-unit, and the connectivity is *L*-type. Furthermore, these *L*-type units are condensed by sharing triangular faces via M1 and M3 sites to form a 3D icosahedral network. The linkage between the two *L*-type units constitutes a *B*-type (bridge-type) connection (highlighted in Fig. 7c). In addition, each *L*-type unit also generates a pyrochlore-type unit, *i.e.*, four octahedra share their vertices and faces with the central octahedron, located at the center (void) of the *L*-type unit, as shown in Fig. 7b. It is noteworthy that the structure of Mn_3Al_{10} consists of only *B*- and *I*-type of *I*3-cluster connectivities [23]. Additionally, two Zn2 centered icosahedra, which

Table 4. Selected interatomic distances for crystal **I** (< 3.1 Å).

Atom	Distances			Atom	Distances			Atom	Distances		
Zn1	−M4	2.531(1)	6×	M2	−Zn2	2.676(3)	3×	M5	−Zn2	2.479(1)	2×
	−Zn3	2.837(1)	6×		−M4	2.743(1)	3×		−M3	2.754(2)	2×
					−M6	2.853(2)	3×		−M6	2.823(2)	2×
Zn2	−M5	2.479(1)	2×		−Zn3	2.905(3)	3×		−M5	2.852(2)	2×
	−M4	2.503(2)	1×						−M4	2.883(2)	2×
	−M1	2.538(1)	1×	M3	−M1	2.683(1)	1×		−M3	2.894(2)	2×
	−Zn2	2.671(1)	2×		−Zn2	2.741(2)	1×				
	−M2	2.676(3)	1×		−Zn2	2.751(1)	2×	M6	−Zn2	2.713(2)	2×
	−M6	2.713(1)	2×		−M5	2.754(2)	2×		−Zn3	2.814(2)	2×
	−M3	2.741(2)	1×		−M3	2.818(1)	2×		−M5	2.823(2)	2×
	−M3	2.751(1)	2×		−M6	2.851(2)	1×		−M3	2.851(2)	1×
					−M5	2.894(2)	2×		−M2	2.853(2)	1×
Zn3	−M4	2.679(2)	1×		−M3	3.030(1)	2×		−M4	2.866(1)	2×
	−Zn3	2.759(1)	2×						−M6	2.882(2)	2×
	−M6	2.814(2)	2×	M4	−Zn2	2.503(2)	1×				
	−M4	2.821(1)	2×		−Zn1	2.531(1)	1×				
	−Zn1	2.837(1)	1×		−Zn3	2.679(2)	1×				
	−M2	2.905(3)	1×		−M2	2.743(1)	1×				
	−Zn3	2.963(1)	2×		−Zn3	2.821(1)	2×				
					−M4	2.847(2)	2×				
M1	−Zn2	2.538(1)	6×		−M6	2.866(1)	2×				
	−M3	2.683(1)	6×		−M5	2.883(2)	2×				

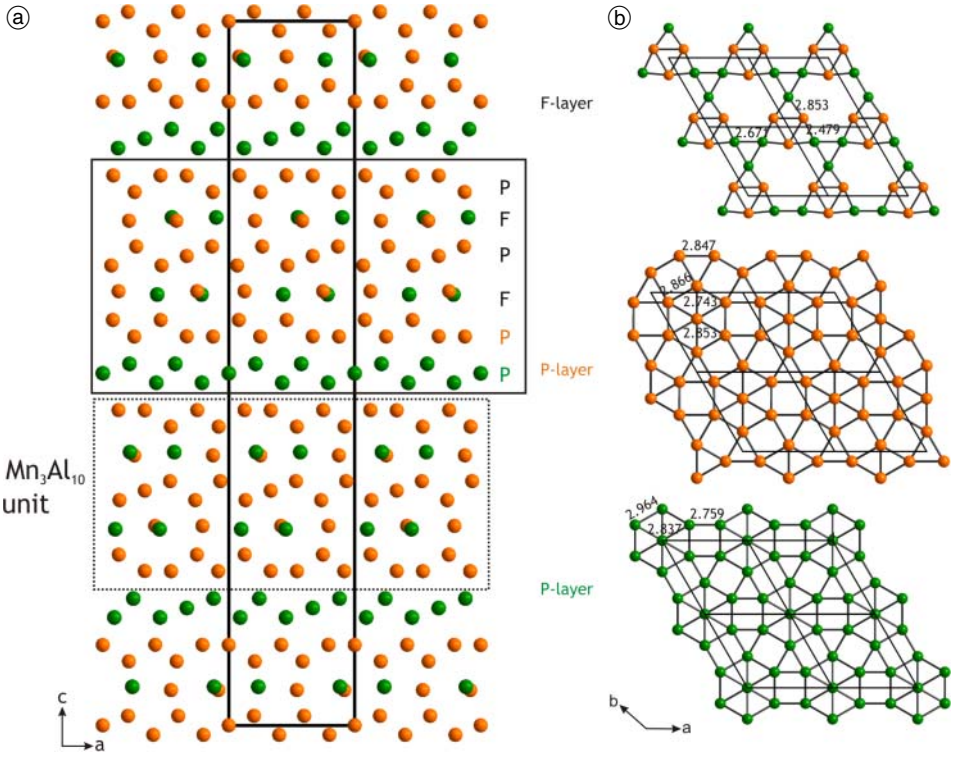

Fig. 5. **(a)** Projection of the unit cell of $Zn_{13}(Cr_xAl_{1-x})_{27}$ along the *c*-axis. The repeating unit $\cdots PFPFPP \cdots$ is highlighted (solid line). The substructure of $Zn_{13}(Cr_xAl_{1-x})_{27}$ shows close resemblance with the Mn_3Al_{10} structure type (dotted line). **(b)** A projection showing the arrangement of atoms in the *F*-, *P*- and *P*-layers perpendicular to the *c*-axis. The *F*-layers are formed by M (orange) and Zn (green) atoms, where as the *P*-layers consist of either M or Zn atoms, only.

are located on an *F*-layer, interpenetrate each other along their pseudo-$\bar{5}$-axes, and they share a common bicapped pentagonal prism centered by M5 atoms, as depicted in Fig. 7d.

Electronic structure

TB-LMTO-ASA calculations were performed on the stoichiometric "$Cr_9Al_{18}Zn_{13}$" as a representative composition of the title compounds with the M1, M2, and M3 sites assigned to Cr atoms and the M4, M5, and M6 sites assigned to Al atoms. Although crystallographic refinement suggested statistical mixing of Cr and Al atoms on all M1–M6 sites, the numerical values of the sof's of the M1–M3 sites slightly preferred Cr occupation. To understand any site preference of Cr and Al atoms among M3–M6 positions (all Wyckoff sites, 18*h*), different models of "$Cr_9Al_{18}Zn_{13}$" were constructed and their total energies were compared. To conduct this comparison, the Wigner-Seitz radii for Cr and Al were kept constant for the different models. Among four different models, placing Cr atoms at M3 or M5 sites gives the lowest total energies compared to Cr atoms located at M4 or M6 sites. The energy difference between the two preferred structural models, *i.e.*, Cr at M3 or M5 is ca. 45.5 meV/fu, slightly in favor of Cr atoms situated at the M3 sites (NOTE: our study here is not exhaustive, but representative). The calculated total DOS and crystal orbital Hamilton population (−COHP) curves are shown in Fig. 8. Analysis of the electronic DOS curve shows that the contribution to total DOS at the Fermi level (134 e^-) arises mostly from chromium 3*d* orbitals, and to a small extent from Al 3*p* orbitals. In addition, the Zn 3*d* orbitals form a narrow band ca. 10 eV below this calculated Fermi level, and are not illustrated. The chromium 3*d* orbitals spread into a band of ca. 10 eV width centered near the calculated Fermi level, and are also split into bonding and antibonding states at the Fermi level (see below).

A quantitative bonding analysis of the $Zn_{13}(Cr_xAl_{1-x})_{27}$ structure using "$Cr_9Al_{18}Zn_{13}$" with Cr atoms at the M3 sites has also been carried out based on the −COHP curves and the corresponding integrated −COHP (−ICOHP)

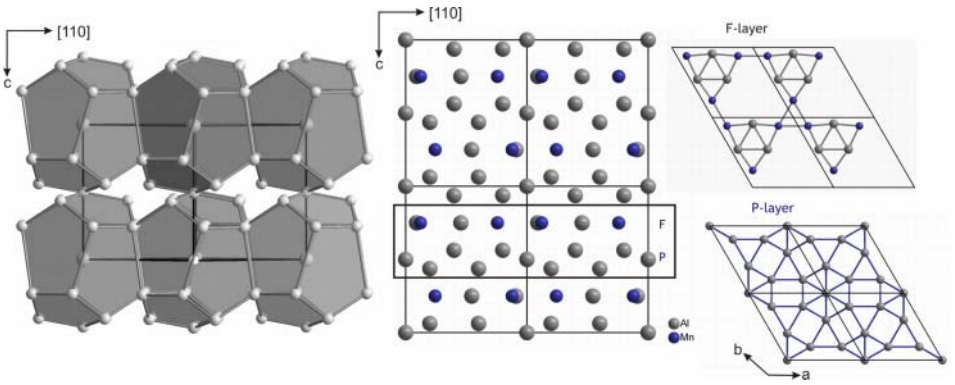

Fig. 6. (Left) [100] Projection of the structure of Mn_3Al_{10} emphasizing condensed polyhedra. (Right) [100] Projection showing the arrangement of atoms in the *F*- and *P*-layers perpendicular to the *c*-axis.

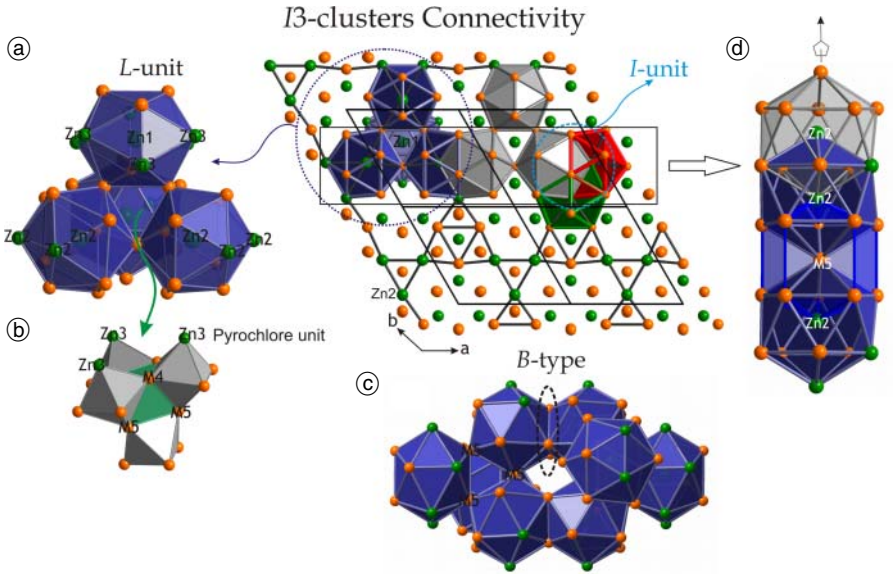

Fig. 7. Different types of *I*3-clusters in the $Zn_{13}(Cr_xAl_{1-x})_{27}$ structure. (**a**) Four vertex-connected icosahedra forming an *L*-type connection. (**b**) A pyrochlore-type unit; a group of four octahedra sharing faces with the central octahedron located at the center of the *L*-unit. (**c**) Condensation of *L*-units along the *c*-direction displaying *B*-type connections. (**d**) Three icosahedra centered by Zn2 atoms displaying a pseudo 5-fold symmetry along the *a*-axis.

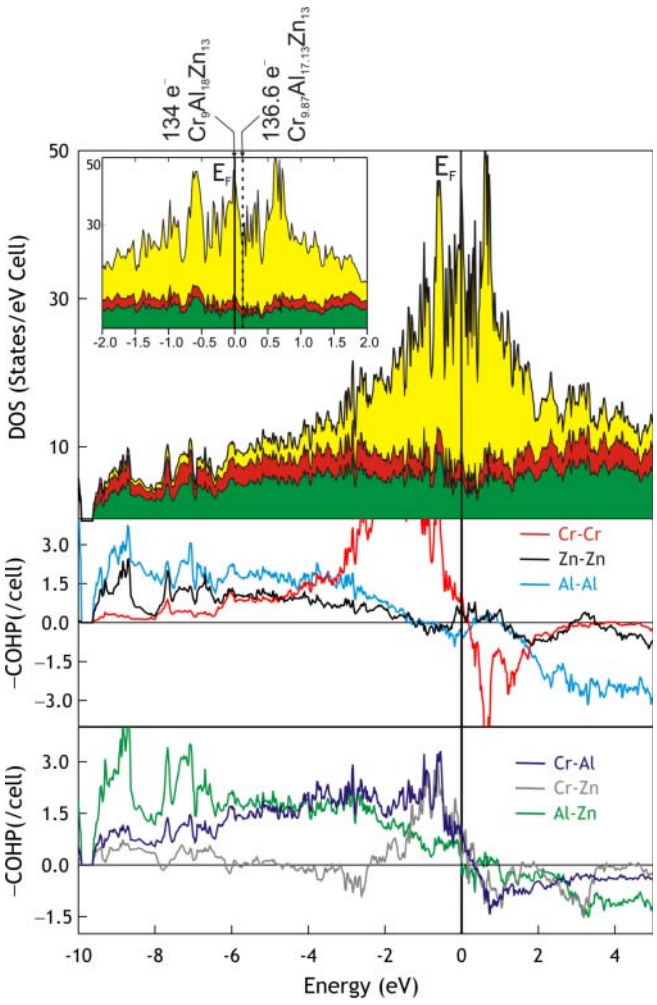

Fig. 8. TB-LMTO-ASA DOS and −COHP curves for "$Cr_9Al_{18}Zn_{13}$" as a model of the $Zn_{13}(Cr_xAl_{1-x})_{27}$ structure. In the DOS curve, partial atomic contributions, Al (green), Zn (red), and Cr (yellow), are indicated. The solid line at 0 eV (134 e^-) denotes the Fermi level, and dotted line at 0.12 eV (136.6 e^-) in the inset corresponds to upper composition limit of this phase. In the −COHP curves, positive values are bonding interactions; negative values are antibonding interactions.

Table 5. −ICOHP values for various interatomic contacts (<3.1 Å) in "$Cr_9Al_{18}Zn_{13}$".

Interaction	*d*/Å	−ICOHP/eV/bond	No. of interactions (*n*)
Cr−Cr	2.694–3.033	2.62	11
Zn−Zn	2.690–2.968	2.53	13
Al−Al	2.835–2.897	4.60	18
Cr−Al	2.749–2.914	4.90	11
Cr−Zn	2.586–2.909	2.48	15
Al−Zn	2.481–2.834	7.12	11

values, which are measures of relative bond indices and listed in Table 5. In "$Cr_9Al_{18}Zn_{13}$", the strongest orbital interactions are found for Zn−Al, Cr−Al and Al−Al contacts, whose −ICOHP values, respectively, are 7.12, 4.90, and 4.60 eV/bond. This shows that both homo- and heteronuclear interactions are responsible for the stability of the new phase. According to the −COHP curves, the Zn−Zn and Zn−Al interactions are optimized: bonding orbitals are filled; antibonding orbitals are empty. In addition, the Zn−Zn, Al−Al and Cr−Zn contacts show non-bonding character, whereas Cr−Cr bonding changes sharply around the Fermi level from bonding to antibonding character. Moreover, optimization of heteronuclear Cr−Al, Zn−Al, and Cr−Zn interactions take place at ca. 0.12 eV above the Fermi level, which corresponds to 138 e^- per formula unit. This suggests a small homogeneity range for the new phase, and is close to the upper limit of Cr/Al substitution that emerged from our single crystal diffraction studies: $Zn_{13}Cr_{9.87}Al_{17.13}$ gives 136.6 valence electrons.

Conclusions

The new phases $Zn_{13}(Cr_xAl_{1-x})_{27}$ ($x = 0.34–0.37$) were successfully synthesized with maximum yield. According to single crystal diffraction studies, the new phase crystal-

lizes in a rhombohedral system and adopts a new structure type. Combined single crystal and powder X-ray diffraction experiment revealed that the title phase coexist with Cr_5Al_8 and $(Cr,Al)_3Zn$, depending upon the reaction condition. The main building block of new structure is a three vertex connected icosahedra, known as the *I*3 cluster, showing *L*-type, *B*-type, and *I*-type connectivities reflecting complexity of the new phase. The electronic structure calculation and bonding analysis indicated that heteroatomic Cr−Zn, Cr−Al, and Zn−Al bonding are the strongest, which is optimized for these valence electron counts.

Acknowledgments. This work was carried out at the Ames Laboratory, which is operated for the U.S. Department of Energy by Iowa State University under Contract No. DE-AC02-07CH11358. This work was supported by the Materials Sciences Division of the Office of Basic Energy Sciences of the U.S. Department of Energy.

References

[1] Shechtman, D.; Blech, I.; Gratias, D.; Cahn, J. W.: Metallic phase with long-range orientational order and no translational symmetry. Phys. Rev. Lett. **53** (1984) 1951–1953.
[2] Steurer, W: Twenty year of structure research on quasicrystals. Part I. Pentagonal, octagonal, decagonal and dodecagonal quasicrystals. Z. Kristallogr. **219** (2004) 391–446
[3] Tsai, A.-P.: "Back to the future"-An account discovery of stable quasicrystals. Acc. Chem. Res. **36** (2003) 31–38.
[4] Bergman, G.; Waugh, J. L. T.; Pauling, L.: The crystal structure of the metallic phase $Mg_{32}(Al, Zn)_{49}$. Acta Cryst. 10 (1957) 254–259.
[5] Mackay, A. L.: A dense non-crystallographic packing of equal spheres. Acta Crystallogr. **15** (1962) 916–918.
[6] Tsai, A.-P.; Guo, J. Q.; Abe, E.; Takakura, H.; Sato, T. J.: Alloys: A stable binary quasicrystal. Nature **408** (2000) 537–538
[7] Tsai, A.-P.: A test of Hume-Rothery rules for stable quasicrystals. J. Non-Crystalline Solids **334&335** (2004) 317–322.
[8] Trambly de Laissardière, G.; Nguyen-Manh, D; Mayou, D.: Electronic structure of complex Hume-Rothery phases and quasicrystals in transition metal aluminides. Prog. Mater. Sci. **50** (2005) 679–788.
[9] Mizutani, U.; Takeuchi, T.; Sato, H.: Interpretation of the Hume–Rothery rule in complex electron compounds: γ-phase Cu_5Zn_8 Alloy, FK-type $Al_{30}Mg_{40}Zn_{30}$ and MI-type $Al_{68}Cu_7Ru_{17}Si_8$ 1/1–1/1–1/1 approximants. Prog. Mater. Sci. **49** (2004) 227–261.
[10] Berger, R. F.; Lee, S.; Johnson, J.; Nebgen, B.; So, A.C.Y.: Laves phases, γ-brass, and 2×2×2 superstructures: A new class of quasicrystal approximants and the suggestion of a new quasicrystal. Chem. Eur. J. **14** (**2008**) 6627–6639.
[11] Berger, R. F.; Lee, S.; Johnson, J.; Nebgen, B.; Sha, F.; Xu, J.: The mystery of perpendicular 5-fold axes and the fourth dimension in intermetallic structures. Chem. Eur. J. **14** (2008) 3908–3930.
[12] Pey Gómez, C.; Lidin, S.: Superstructure of Eu_4Cd_{25}: A quasicrystal approximant. Chem. Eur. J. **10** (2004) 3279–3285.
[13] Takakura, H.; Pey Gómez, C.; Yamamoto, A.; De Boissieu, M.; Tsai, A.-P.: Atomic structure of the binary icosahedral Yb−Cd quasicrystal. Nature Materials **6** (2007) 58–63.
[14] Pey Gómez, C.; Lidin, S.: Structure of $Ca_{13}Cd_{76}$: A novel approximant to the $MCd_{5.7}$ quasicrystals (M = Ca, Yb). Angew. Chem. Int. Edn. **40** (2001) 4037–4039.
[15] Ohashi, W.; Spaepen, F.: Stable Ga−Mg−Zn quasi-periodic crystals with pentagonal dodecahedral solidified morphology. Nature **330** (1987) 555–556.
[16] Lin, Q.; Corbett, J. D.: The 1/1 and 2/1 approximants in the ScMgZn quasicrystal system: Triacontahedral clusters as fundamental building blocks. J. Am. Chem. Soc. **128** (2006) 13268–13273.
[17] Sato, T. J.; Takakura, H.; Tsai, A.-P.; Shibata, K.: Anisotropic spin correlations in the Zn-Mg-Ho icosahedral quasicrystal. Phys. Rev. Lett. **81** (1998) 2364–2367.
[18] Lin, Q.; Corbett, J. D.: Development of the Ca−Au−In icosahedral quasicrystal and two crystalline approximants: practice via pseudogap electronic tuning. J. Am. Chem. Soc. **129** (2007) 6789–6797.
[19] Audier, M.; Durand-Charre, M.; Laclau, E.; Klein, H.: Phase equilibria in the Al−Cr system. J. Alloys Comp. **220** (1995) 225–230.
[20] Grushko, B.; Przepiórzyński, B.; Pavlyuchkov, D.: On the constitution of the high-Al region of the Al−Cr alloy system. J. Alloys Comp. **454** (2008) 214–220.
[21] Mahdouk, K.; Gachon, J.-C.: Thermodynamic investigation of the aluminum-chromium system. J. Phase Equilibria. **21** (2000) 157–166.
[22] Cao, B. B.; Kuo, K. H.: Crystal structure of the monoclinic η-$Al_{11}Cr_2$. J. Alloys Comp. **458** (2008) 238–247.
[23] Kreiner, G.; Franzen, H. F.: A new cluster concept and its application to quasi-crystals of the i-AlMnSi family and closely related crystalline structures. J. Alloys Comp. **221** (1995) 15–36.
[24] Deng, D. W.; Mo, Z. M.; Kuo, K. H.: Crystal structure of the orthorhombic Al_4(Cr,Fe) approximant of the Al−Cr−Fe decagonal quasicrystal. J. Phys.: Condens. Matter. **16** (2004) 2283–2296.
[25] Schenk, T.; H. Klein, H.; Audier, M.; Simonet, V.; Hippert, F.; Rodriguez-Carvajal, J.; Bellissent, R.: Structure and magnetism of the μ-$Al_4Mn_xCr_{1-x}$ approximant phase ($0 \le x \le 1$). Philos. Mag. Lett. **76** (1997) 189–198.
[26] Deng, D. W; Kuo, K. H.: Crystal structure of the b.c.o. Al_4(Cr,Ni) decagonal approximant. J. Alloys Comp. **342** (2002) 101–104.
[27] Mo, Z. M.; Zhou, H. Y.; Kuo, K. H.: Structure of υ-$Al_{80.61}Cr_{10.71}Fe_{8.68}$, a giant hexagonal approximant of a quasicrystal determined by a combination of electron microscopy and X-ray diffraction. Acta Cryst. B **56** (2000) 392–401.
[28] Reumont, G.; Perrot, P.: Thermodynamic assessment of the zinc-rich part of the Cr−Zn system: J. Phase Equilibria **24** (2003) 50–54.
[29] Su, X.; Liu, Y.; Liu, Y. H. D.; Tedenac, J.-C.; Yin, F.; Wang, J.: Experimental investigation and thermodynamic assessment of the Zn−Cr system. J. Alloys Comp. **496** (2010) 159–163.
[30] Hanemann H.: Bemerkung zum system zink-chrom, Z. Metallkd. **32** (1940) 91–92.
[31] R. Fourmentin; G. Reumont; P. Perrot; B. Gay; S. Claessens: Le diagramme Al−Cr−Zn à 460 °C. J. Phys. IV France **113** (2004) 65–68.
[32] Brown, P. J.: The Structure of the ζ-Phase in the Transition Metal-Zinc Alloy Systems, Acta Crystallogr. **15** (1961) 608–612.
[33] Fourmentin, R.; Avettand-Fènoël, M.-N.; Reumont, G.; Perrot, P.: Optimization of the Al−Cr−Zn system at 460 °C. J. Mater. Sci. **42** (2007) 7934–7938.
[34] Thimmaiah, S; Miller, G. J.: On the structural chemistry of γ-brasses: Two different interpenetrating networks in ternary F-cell Pd−Zn−Al phases. Chem. Eur. J. **16** (2010) 5461–5471.
[35] Ko, H.; Gourdon, O.; Gout, D.; Mun, E.-D.; Thimmaiah, S.; Miller, G. J.: Rhombohedrally distorted γ-brasses $Cr_{1-x}Fe_xGa$. Inorg. Chem. **49** (2010) 11505–11515.
[36] Gourdon, O.; Bud'ko, S. L.; Williams, D.; Miller, G. J.: Crystallographic, electronic, and magnetic studies of ζ_2-GaM (M = Cr, Mn or Fe): Trends in itinerant magnetism. Inorg. Chem. **43** (2004) 3210–3218.
[37] *SMART* (5.632); Bruker AXS, Inc.; Madison, WI (1997).
[38] Stoe & Cie GmbH: *X-SHAPE* (2.07). Crystal Optimization for Numerical Absorption Correction. Darmstadt (Germany), 2005.
[39] Stoe & Cie GmbH: *X-RED* (1.31). Data Reduction Program. Darmstadt (Germany), 2005.
[40] *SHELXTL* (6.14); Bruker ASX, Inc.: Madison, WI, (2000).
[41] Farrugia, L. J.: WinGX suite for small-molecule single-crystal crystallography. J. Appl. Crystallogr. **32** (1999) 837–838.
[42] Andersen, O. K.: Linear methods in band theory. Phys. Rev. B **12** (1975) 3060–3083.
[43] Andersen, O. K.; Jepsen, O.: Explicit, first-principles tight-binding theory. Phys. Rev. Lett. **53** (1984) 2571–2574
[44] Andersen, O. K; Jepsen, O.; Glötzel, D.: in Highlights of Condensed Matter Theory (Eds.: Bassani, F.; Fumi, F; Tosi, M. P.), North-Holland, New York, 1985.

[45] Andersen, O. K.; Pawlowska, Z.; Jepsen, O.: Illustration of the linear-muffin-tin-orbital tight-binding representation: Compact orbitals and charge density in Si. Phys. Rev. B **34** (1986) 5253–5269.
[46] von Barth, U.; Hedin, L.: A local exchange-correlation potential for the spin polarized case. J. Phys. C: Solid State Phys. **5** (1972) 1629–1642.
[47] Koelling, D. D.; Harmon, B. N.: A technique for relativistic spin-polarised calculations. J. Phys. C: Solid State Phys. **10** (1977) 3107–3114.
[48] Jepsen, O.; Andersen, O. K.: Calculated electronic structure of the sandwichd1 metals LaI_2 and CeI_2: Application of new LMTO techniques. Z. für Physik B Condensed Matter. **97** (1995) 35–47.
[49] Dronskowski, R.; Blöchl, P.: Crystal orbital Hamilton populations (COHP): energy-resolved visualization of chemical bonding in solids based on density-functional calculations. J. Phys. Chem. **97** (1993) 8617–8624.
[50] Blöchl, P. E.; Andersen, O. K.; Jepsen, O.: Improved tetrahedron method for Brillouin-zone integrations. Phys. Rev. B **49** (1994) 16223–16233.
[51] Kreiner, G.; Franzen, H. F.: The crystal structure of λ-Al_4Mn. J. Alloys Comp. **261** (1997) 83–104.
[52] Li, X. Z.; Hiraga, K.; Yamamoto, A.: Icosahedral cluster in the structure of an Al−Cr−Ni κ-phase. Phil. Mag. A **76** (1997) 657–666.
[53] Kreiner, G.; Moguilnikov, Y.; Burkhardt, U.; Schäpers, M.: Hume-Rothery controlled formation of structurally complex alloy phases in the ternary Ga–Mg–Pd system. J. Non-Crystalline Solids **334&335** (2004) 17–22.
[54] Kudla, C.; Prots, Y.; Leineweber, A.; Kreiner, G.: On the crystal structure of γ-AgMg4. Z. Kristallogr. **220** (2005) 102–114.
[55] Katrych, S.; Gramlich, V.; Steurer, W.: Trigonal Ir_9Al_{28}, a new structure type and approximant to decagonal quasicrystals. J. Alloys Comp. **407** (2006) 132–140.